Available online at www.sciencedirect.com
ScienceDirect
Journal of Power Sources 169 (2007) 110–116
JOURNAL OF POWER SOURCES
www.elsevier.com/locate/jpowsour

Catalytic processes during preferential oxidation of CO in H_2-rich streams over catalysts based on copper–ceria☆

D. Gamarra[a], A. Hornés[a], Zs. Koppány[b], Z. Schay[b], G. Munuera[c], J. Soria[a], A. Martínez-Arias[a,*]

[a] *Instituto de Catálisis y Petroleoquímica, CSIC, C/Marie Curie 2, Campus Cantoblanco, 28049 Madrid, Spain*
[b] *Institute of Isotopes, Hungarian Academy of Sciences, H 1525-Budapest, Hungary*
[c] *Departamento de Química Inorgánica e Instituto de Ciencia de Materiales (Centro Mixto Universidad de Sevilla-CSIC), 41092 Sevilla, Spain*

Available online 30 January 2007

Abstract

Nanostructured catalysts based on combinations between oxidised copper and cerium entities prepared by two different methods (impregnation of ceria and coprecipitation of the two components within reverse microemulsions) have been examined with respect to their catalytic performance for preferential oxidation of CO in a H_2-rich stream (CO-PROX). Correlations between their catalytic and redox properties are established on the basis of parallel analyses of temperature programmed reduction results employing both H_2 and CO as reactants as well as by XPS. Although general catalytic trends can be directly correlated with the redox properties observed upon separate interactions with each of the two reductants (CO and H_2), the existence of interferences between both reductants must be considered to complete details for such activity/redox correlation. Differences in the nature of the active oxidised copper–cerium contacts present in each case determine the catalytic properties of these systems for the CO-PROX process.

Keywords: CuO/CeO_2; CO-PROX; H_2-TPR; CO-TPR; XPS; Microemulsion

1. Introduction

Production of H_2 for polymer fuel cells (PEMFC) is usually accomplished by a multi-step process that includes catalytic reforming of hydrocarbons or oxygenated hydrocarbons followed by water gas-shift (WGS) [1,2]. The gas stream obtained after these processes presents in most cases a relatively high CO concentration that disallows efficient handling of the fuel by the Pt alloy anode usually employed in the PEMFC. Preferential (or selective) oxidation of CO (CO-PROX process) has been recognized as one of the most straightforward and cost-effective methods to achieve acceptable CO concentrations (below ca. 100 ppm) [3–8]. Among different types of catalysts that have shown their ability for this process (including those based on Pt and Au), a group constituted by catalysts based on closely interacting copper oxide and ceria (or structurally related cerium-containing mixed oxides) has shown promising properties in terms of activity, selectivity and resistance to CO_2 and H_2O, while their lower cost could make them strongly competitive [3,4,6,7,9–15].

The particular ability of the latter class of catalysts for the CO-PROX or related processes has been essentially attributed to the synergistic redox properties in the presence of copper–ceria interfacial sites [4,6,10,11,16–21]. Previous work from our group was dedicated to analyse differences in the CO-PROX catalytic performances as a function of the support employed in a series of $CuO/(Ce,M)O_x$ (with M = Zr or Tb) catalysts [11]. In agreement with studies of a similar type [9,22,23], it was shown that the CuO/CeO_2 configuration yielded best results in terms of both CO conversion and CO-PROX selectivity, which was generically attributed to the higher interfacial redox activity of such catalyst [11]. Selectivity differences between the catalysts could be related to structural/morphological properties of the copper oxide species present in each case [11]. Nevertheless, details are lacking with respect to the nature of the processes involved in the reaction mechanism and/or their respective evolutions during the catalytic process [6,10,16]. Generally speaking, the properties of

☆ This paper presented at the 2nd National Congress on Fuel Cells, CONAPPICE 2006.

* Corresponding author. Tel.: +34 915854940; fax: +34 915854760.
E-mail address: amartinez@icp.csic.es (A. Martínez-Arias).

0378-7753/$ – see front matter © 2007 Elsevier B.V. All rights reserved.
doi:10.1016/j.jpowsour.2007.01.048

copper entities for CO oxidation promotion apparently depend strongly on their dispersion degree and/or related degree of interaction with ceria [11,16,17,24]. Additionally, incorporation of copper into the fluorite network of ceria can induce important modifications on its chemical properties [25–28].

Within this context, the present work aims to get further insights into the catalytic properties of catalysts based on combinations between copper and cerium oxides for CO-PROX. Focus will be put in this case on analysing the correlations between catalytic and redox properties of this type of systems. For this purpose, two series of catalysts differing in the preparation method and copper loading employed, in order to have well differentiated catalysts configurations [27,29], have been examined with respect to their catalytic performance for the CO-PROX process and explored in parallel with respect to their redox properties by means of H_2-TPR, CO-TPR and XPS.

2. Experimental

Two Cu-doped ceria samples, labelled as $Ce_{1-x}Cu_xO_2$ ($x = 0.05$ and 0.2) were prepared with a modified reverse microemulsion method [27,30]. Briefly, the precursors were introduced in a reverse microemulsion (water in oil) using *n*-heptane as the organic phase, Triton X-100 (Aldrich) as surfactant, and hexanol as cosurfactant. Then, this suspension was mixed with another similar suspension containing as aqueous phase an alkali solution (TMAH, Aldrich) in order to coprecipitate the cations. The resulting mixtures were stirred for 24 h, centrifuged, decanted, and rinsed with methanol. Finally, the solid portion was dried overnight at 373 K, and the resulting powders were calcined under air at 773 K for 2 h.

Two samples of copper supported on CeO_2 (Cu wt% of 1.0 and 5.0, denoted as $1CuO/CeO_2$ and $5CuO/CeO_2$, respectively) were prepared by incipient wetness impregnation of a CeO_2 support prepared by microemulsion (in a similar manner as described above; it displayed specific surface area – S_{BET} – of 130 $m^2\,g^{-1}$ after calcination at 773 K) with copper nitrate aqueous solutions. Following impregnation, the samples were dried overnight at 373 K and finally calcined under air at 773 K for 2 h.

The catalysts calcined in situ (under oxygen diluted in Ar at 773 K) were tested in a glass tubular catalytic reactor for their activity under an atmospheric pressure flow (using mass flow controllers to prepare the reactant mixture) of 1% CO, 1.25% O_2 and 50% H_2 (Ar balance), at a rate of 1×10^3 $cm^3\,min^{-1}\,g^{-1}$ (roughly corresponding to 80,000 h^{-1} GHSV) and using a heating ramp of 5 K min^{-1} up to 523 K. Analysis of the feed and outlet gas streams was done by gas infrared (Perkin-Elmer FTIR spectrometer model 1725X, coupled to a multiple reflection transmission cell–Infrared Analysis Inc. "long path gas minicell", 2.4 m path length, ca. 130 cm^3 internal volume) while a paramagnetic analyser (Servomex 540 A) was used to analyse the O_2 concentration. No products other than those resulting from CO or H_2 combustion (i.e. CO_2 and H_2O; only a residual contribution of possible WGS or reverse WGS reactions, taking place in any case at temperatures higher than ca. 453 K, was estimated from mass balance under the conditions employed; this was also confirmed by independent tests including CO_2 or H_2O as reactants) were detected in the course of the runs, in agreement with previous results on catalysts of this type [6,10,12,24]. On this basis, values of percentage conversion and selectivity in the CO-PROX process are defined as:

$$X_{O_2} = \frac{F^{in}_{O_2} - F^{out}_{O_2}}{F^{in}_{O_2}} \times 100; \qquad X_{CO} = \frac{F^{in}_{CO} - F^{out}_{CO}}{F^{in}_{CO}} \times 100;$$

$$S_{CO_2} = \frac{X_{CO}}{2.5X_{O_2}} \times 100$$

where X and S are the percentage conversion and selectivity, respectively, and F is the (inlet or outlet) molar flow of the indicated gas.

Temperature programmed reduction (TPR) was measured in a flow system using 1%H_2/Ar and 5%CO/He premixed gases with flow rates of 30 and 40 mL min^{-1}, respectively. A cold trap filled with liquid nitrogen was placed after the reactor to remove water. The system was equipped with a thermal conductivity detector and a Balzers PRISMA QMS coupled via an UHV dosing valve. About 40 mg catalyst was placed into a quartz U-tube and calcined in 5%O_2/He at 773 K for 1 h using 40 mL min^{-1} flow rate and 10 K min^{-1} ramp. The sample was cooled to room temperature, purged with Ar and after switching to the reducing gas mixture it was heated to 773 K using 10 K min^{-1} ramp. Due to the uncontrolled flow conditions and the manual setting of the dosing valve the QMS signal cannot be quantified.

X-ray photoelectron spectra (XPS) were recorded with a Leybold–Heraeus spectrometer equipped with an EA-200 hemispherical electron multichannel analyser (from Specs) and a 120 W, 30 mA Mg Kα X-ray source. The samples (0.2 mg) were slightly pressed into a small (4 mm × 4 mm) pellet and then mounted on the sample rod and introduced into the pretreatment chamber where it could be subjected to thermal or redox treatments under ca. 1 Torr of reactive gases. Reduction upon Ar^+-etching treatments was carried out with a current of 6 mA and an acceleration voltage of 3.5 kV (ion current, 8 μA). Following each treatment, the sample was moved into the ion-pumped analysis chamber where it was further outgassed until a pressure less than 2×10^{-9} Torr was attained (2–3 h). This low pressure was maintained during all the data acquisition by ion pumping of the chamber. After each treatment, XP spectra in the relevant energy windows were collected for 20–90 min, depending on the peak intensities, at a pass energy of 44 eV (1 eV = 1.602×10^{-19} J) which is typical of high resolution conditions. The intensities were estimated by calculating the integral of each peak after subtraction of an S-shaped Shirley-type background with the help of UNIFIT for Windows (Version 3.2) software [31]; atomic ratios were then derived using the appropriate experimental sensitivity factors. All binding energies (BE) were referenced to the adventitious C1s line at 284.6 eV. This reference gave BE values with an accuracy of ±0.1 eV; the peak u''' characteristic of Ce^{4+} was thus obtained at 917.0 ± 0.1 eV. In the case of Ce(3d) spectra, factor analysis (FA) was used to calculate the Ce^{3+}/Ce^{4+} ratios in each set of spectra recorded, using the methodology developed in a previous work [32].

Table 1
Main textural and structural characteristics of the copper–ceria catalysts examined in this work [27,29]

Sample	Specific surface area, S_{BET} ($m^2\ g^{-1}$)	Lattice parameter[a] (Å)	Crystal size (nm)	Phases detected[b]
$1CuO/CeO_2$	107	5.410	7.8	Fluorite CeO_2
$5CuO/CeO_2$	101	5.413	8.1	Fluorite CeO_2, tenorite CuO
$Ce_{0.95}Cu_{0.05}O_2$	130	5.410	7.0	Fluorite $Ce_{1-x}Cu_xO_2$
$Ce_{0.8}Cu_{0.2}O_2$	151	5.413	6.6	Fluorite $Ce_{1-x}Cu_xO_2$

[a] For the fluorite phase.
[b] Based on XRD and Raman [27,29].

3. Results and discussion

The catalysts analysed in this work were characterised in detail in previous articles [27,29]. A brief summary of the results obtained in such articles and which is considered of relevancy to the objectives of the present work is given here for the reader's sake. As collected in Table 1, lattice parameters estimated from XRD are close to that expected for pure ceria for all the samples. It must be however considered that copper introduction into the ceria fluorite lattice is not expected to induce significant changes in this parameter [19,20,26,27,29]. Indeed, analysis of lattice microstrain (derived from XRD results) and Raman results revealed significant differences between samples prepared by impregnation and microemulsion–coprecipitation. These have been related to the fact that, as expected, copper remains essentially at the sample surface in the former samples while copper (at least a part of it) appears to be incorporated into the ceria fluorite lattice in the latter [27,29]. Nevertheless, a certain copper surface segregation, increasing with the copper loading, appears evident in the systems prepared by microemulsion–precipitation, as evidenced mainly by XEDS and Ar^+-sputtering XPS analyses [29]. Therefore, the catalysts of the $Ce_{1-x}Cu_xO_2$ series can be probably better described as $CuO/Ce_{1-z}Cu_zO_2$ (with the amount of segregated CuO increasing with x), since single solid solution of the copper is not fully achieved. In turn, although CuO-type clusters dispersed on the ceria support apparently predominate for the two xCuO/CeO_2 catalysts, differences between them have been shown to be related to the presence of large crystalline CuO particles (evidenced by XRD and electron microscopy [27,29]) in $5CuO/CeO_2$. On the other hand, copper incorporation induces some surface area decrease in the samples prepared by impregnation, probably due to some copper covering of interparticle pores (Table 1). In contrast, the surface area increases with the copper amount for the samples prepared by microemulsion–coprecipitation, in correlation with the mentioned introduction of copper into the ceria lattice and with changes in primary particle sizes (Table 1). Concerning the electronic state of copper, XAFS analyses (in agreement with XPS, as shown below) revealed that it appears in a fully oxidised Cu^{2+} chemical state with relatively small differences (except for the crystalline CuO detected in $5CuO/CeO_2$) between the samples concerning its electronic characteristics [27].

Fig. 1 shows the results obtained for the CO-PROX catalytic activity of the samples. As mentioned in Section 2, basically CO and H_2 combustion are the only reactions taking place under the examined conditions. The overall evolution observed in the CO conversion profile displaying a maximum conversion at intermediate reaction temperature is (as inferred also from analysis of the CO_2 selectivity) a consequence of the competition between both combustion reactions, in accordance with results typically observed for this type of systems [3,4,6,7,9–14]. In this respect, as discussed in more detail elsewhere [13], two regions can be basically differentiated in the activity profiles. A first one at low temperature (<ca. 373 K, where the CO conversion increases) in which CO and H_2 do not compete strongly for the active sites [6,8]. A small promotion of H_2 oxidation in this zone by gaseous CO can result in the low temperature minimum observed in the CO_2 selectivity in some cases [8]. The second region corresponds to high reaction temperature points in which CO and

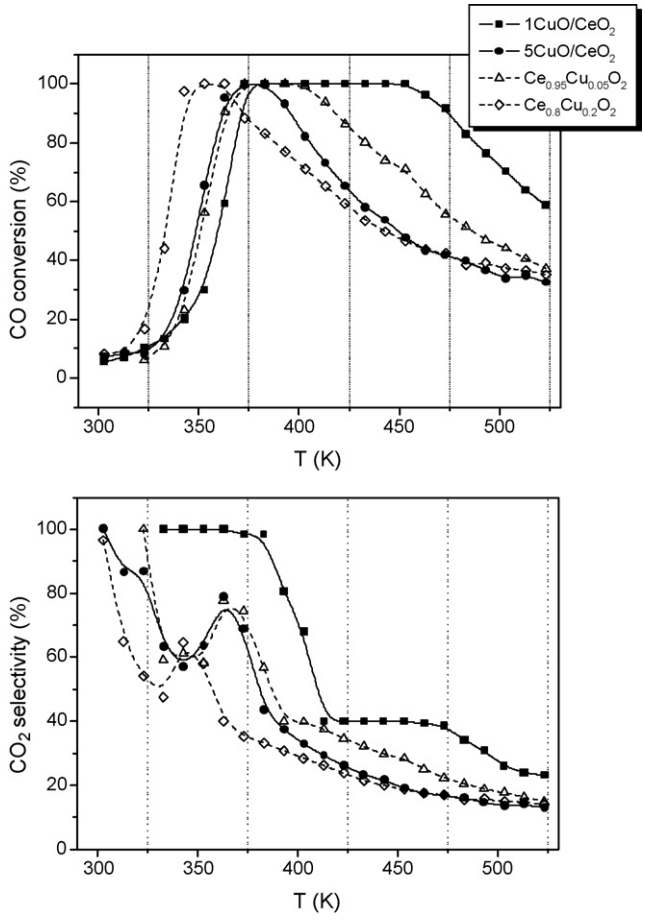

Fig. 1. Catalytic activity under 1% CO, 1.25% O_2 and 50% H_2 (Ar balance) for the indicated catalysts. Top: CO conversion. Bottom: selectivity to CO_2.

H_2 strongly compete for the available active oxygen and which results in the strong high temperature decrease of CO_2 selectivity as a consequence of the significantly higher H_2 partial pressure within a Mars–van Krevelen kinetic scheme [7,13,33].

Appreciable differences are observed between the CO-PROX activity of the catalysts as a function of the copper loading and the preparation method employed. It appears clear that, considering the practical absence of other reactions different than the oxidations of CO and H_2 (as mentioned in Section 2), the oxidation activity of the catalysts (for both reductants) increases with increasing the copper loading in any of the series. Nevertheless, the balance between both oxidation reactions results in increases in CO_2 selectivities with decreasing the copper loading. Among all the examined catalysts, the $1CuO/CeO_2$ apparently results the most interesting from a practical point of view since it achieves full CO conversion at full CO_2 selectivity in a narrow temperature window (of ca. 10 K) slightly above 375 K; a good catalytic behaviour has been also observed for this system in the presence of CO_2 and H_2O in the reactant mixture (although they slightly poison the catalyst) as well as with respect to prolonged aging under the reactant stream, although these analyses are out of the scope of the present study [34].

XPS analysis of the cerium reveals that it displays a fully oxidised state (Ce^{4+}) in the initial calcined samples. The analysis of copper by XPS employing Wagner diagrams (see refs. [35,36] for details) indicates that it appears as fully oxidised Cu^{2+} in the initial calcined samples although the shift of Cu(2p and AES) parameters with respect to those of pure CuO indicates some modifications of its electronic properties which must be related to the size of the particles and their interaction with ceria [20]. Wagner's chemical state plot for the impregnated samples in Fig. 2 shows that copper parameters in sample $1CuO/CeO_2$ fit on the dashed line of slope −3 of bulk CuO, which indicates that this is also the chemical state of the copper in this sample; however, the shift, along this line, from the bulk CuO parameters toward those found for CuO overloaded ZSM-5 zeolites [37] indicates a strong interaction of thin CuO-*like* small clusters with the ceria [38]. Noteworthy, this copper is almost completely reduced to a Cu_2O-*like* phase after 30 min contact with 1 Torr of CO at 373 K (see the shift toward the slope −3 dashed line of bulk Cu_2O in the diagram) while a complete reduction is achieved after 0.5 min of Ar^+-etching together with a deep reduction of the support (ca. 90% Ce^{3+} after 5 min). Reoxidation with 1 Torr of O_2 during 1 h at 473 K of the sample subjected to 10 min of sputtering restores the CuO-*like* chemical state of the copper remaining at the surface as well as the Ce^{4+} oxidation state of ceria. Similar behaviour was observed for $5CuO/CeO_2$ though in this case the copper parameters were closer to those of the bulk CuO used as reference, which is consistent with the presence of big CuO particles poorly interacting with the ceria in agreement with characterization by other techniques (Table 1). In general terms, relatively lower reduction degrees are apparently achieved under similar treatments for the copper in $5CuO/CeO_2$ than in $1CuO/CeO_2$. The set of sputtering treatments for $5CuO/CeO_2$ (0.5–10 min) completely remove the more dispersed phase while it reduces to Cu_2O the big particles that remain at the surface. Reoxidation of these particles at

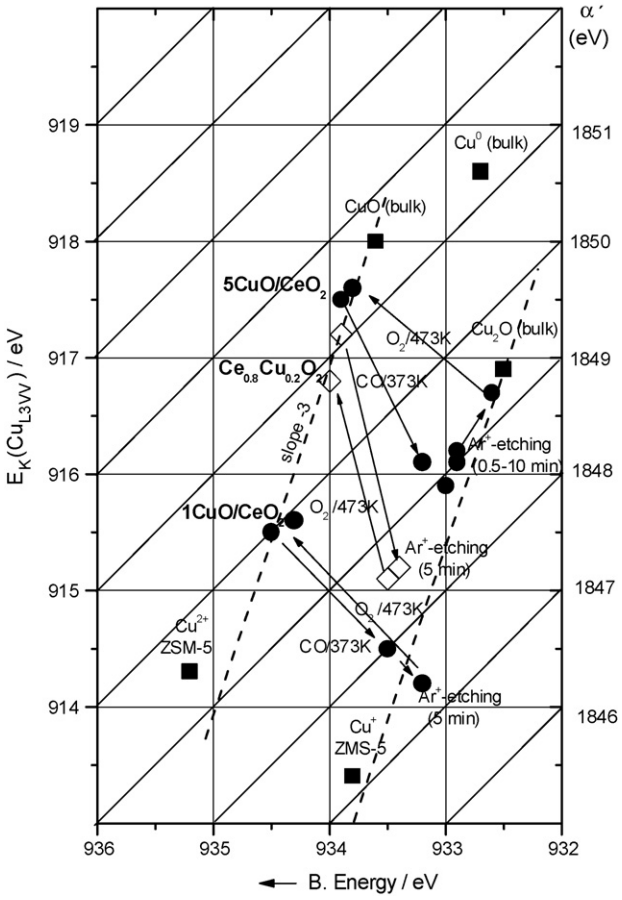

Fig. 2. Wagner plot showing the evolution of Cu (2p and AES) XP parameters during redox treatments performed over the indicated catalysts. Open squares correspond to the $Ce_{0.8}Cu_{0.2}O_2$ sample while full circles correspond to the $1CuO/CeO_2$ or $5CuO/CeO_2$ samples; points for the indicated reference compounds are also included in the plot (as full squares). Note the arrows indicate the various redox treatments performed; these always follow the sequence: CO/373 K–Ar^+-etching–O_2/473 K.

473 K with 1 Torr of O_2 recovers their CuO-*like* chemical state. In the case of the sample $Ce_{0.8}Cu_{0.2}O_2$, the Ar^+ sputtering treatment (0.5–10 min) does not lead to a complete reduction of the copper to Cu^+ probably due to the higher difficulty for reduction of copper incorporated to the fluorite lattice, in agreement with previous investigation [27]. It can be noted that when the data for all the initial samples are compared they fit along the chemical state (slope −3) line for CuO(bulk) but displaced from it (i.e. $5CuO/CeO_2 < Ce_{0.8}Cu_{0.2}O_2 < 1CuO/CeO_2$), which indicates the same chemical state but differences in the size and/or the degree of interaction with the support of the CuO-like phase in the catalysts.

H_2-TPR profiles observed for the catalysts are displayed in Fig. 3. In agreement with XPS results described above and in accordance also with previous work [6,23,32,39], the reduction peaks observed must be attributed to the reduction of copper in the samples although concomitant ceria reduction can also be produced [20,23,39], as also known to occur with other metals [40]. Indeed, quantitative estimation reveal overall H_2 consumptions of 521, 1160, 542 and 1545 μmol per gram of catalyst for $1CuO/CeO_2$, $5CuO/CeO_2$, $Ce_{0.95}Cu_{0.05}O_2$ and

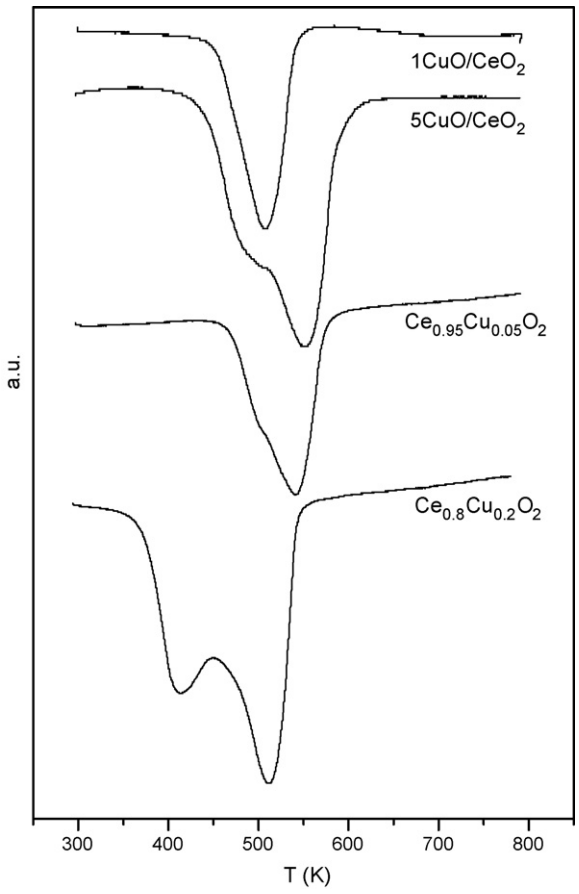

Fig. 3. H_2-TPR profiles obtained for the indicated catalysts.

$Ce_{0.8}Cu_{0.2}O_2$, respectively, which exceed the 157, 787, 297 and 1274 μmol g^{-1}, respectively, required for the reduction of Cu only. Therefore, considering that the copper and cerium must be in fully oxidised states for the initial calcined samples, in accordance to XPS results, ceria reduction apparently also occurs. This appears particularly stronger for the samples prepared by impregnation (and especially for $1CuO/CeO_2$) while it decreases with the amount of copper in any of the two series. This indicates that ceria reduction during the process is mainly favoured by the presence of surface dispersed species. The lower overall relative reduction degrees comparatively achieved for the samples prepared by microemulsion–coprecipitation can also be related with the higher difficulty observed for the reduction of the part of copper introduced into the ceria fluorite structure (Fig. 2) [27]. According to previous results in literature [23,39], and as it has been also observed by us during TPR calibration experiments with pure CuO, the possible sequential reduction of copper ($Cu^{2+} \rightarrow Cu^{+} \rightarrow Cu^{0}$) is difficult to resolve in these experiments, so the different features observed in the samples must be related to structural/morphological differences in the copper oxide entities involved. In this respect, the TPR profiles observed (Fig. 3) clearly reveal the higher copper heterogeneity produced upon increasing the copper loading for any of the two preparation methods employed and in agreement with characterization results described above [27,29].

Thus, the presence of two well-separated reduction peaks in $5CuO/CeO_2$ must be related to the presence of two different copper components in this sample (Table 1). In accordance with previous works [17,39], the component of copper dispersed on ceria (and therefore interacting with it) is responsible of the lowest temperature reduction peak while the peak at highest reduction temperature must be related to the reduction of the well-formed CuO crystals present in this sample. In the case of $Ce_{0.8}Cu_{0.2}O_2$, the presence of two well-separated reduction peaks certainly reflects also the heterogeneity of copper entities present in this sample, as noted above. The lowest temperature reduction peak present in this sample must be due to the reduction of the surface segregated CuO clusters (more easy to be reduced than dispersed copper in $1CuO/CeO_2$, which is likely due to size differences or to different promoting effects by, respectively, CeO_2 and $Ce_{1-z}Cu_zO_2$ mixed oxide acting as support in each case) while the peak at highest reduction temperature must be due to reduction of (at least a part) copper incorporated to the fluorite lattice. This latter component apparently predominate in $Ce_{0.95}Cu_{0.05}O_2$; differences in the respective reduction temperatures for this component between the two $Ce_{1-x}Cu_xO_2$ samples must be related to differences in the oxygen mobilities or promoting effects by previously reduced dispersed entities. In any case, it appears quite interesting that comparison between reduction onsets for the four samples displays (at least qualita-

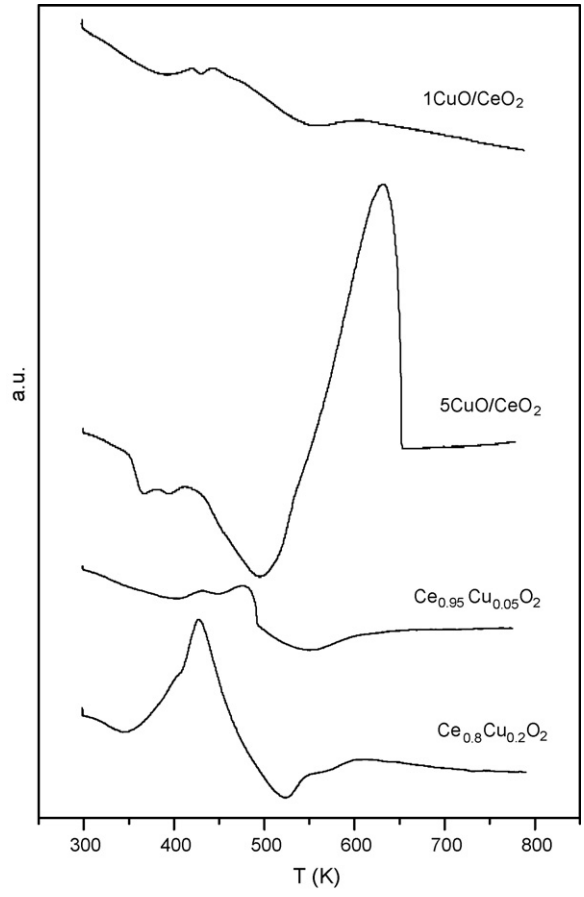

Fig. 4. CO-TPR results obtained for the indicated catalysts with the TCD detector.

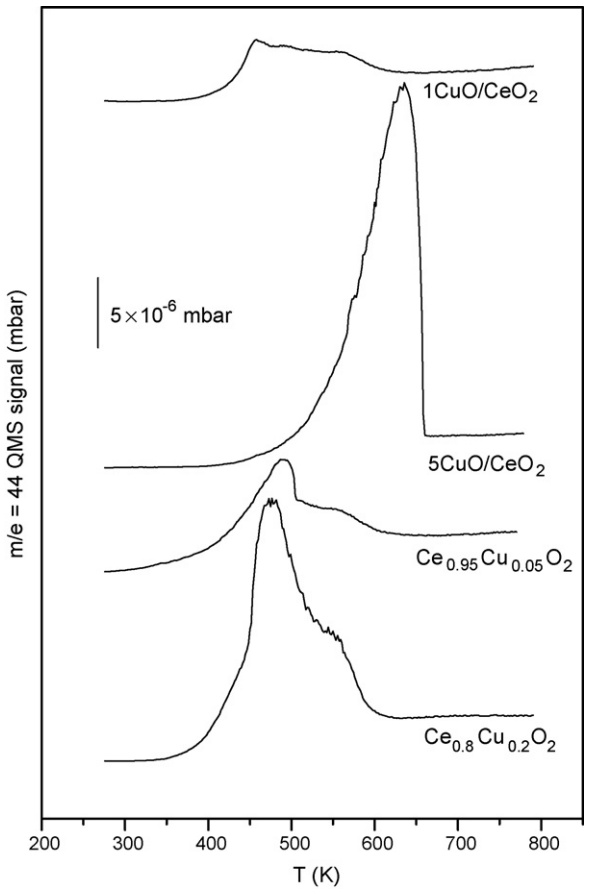

Fig. 5. Evolution of $m/e = 44$ MS signal (corresponding to CO_2) during the CO-TPR experiments for the indicated catalysts.

tively) some agreement with onsets of the highest temperature H_2 oxidation process during the catalytic reactions (Fig. 1). It must be reminded here that a low temperature H_2 oxidation process (responsible of the irregularities observed in the selectivity profiles below ca. 350–380 K) can take place in the presence of CO as a consequence of a promoting effect by gaseous CO [13].

CO-TPR reduction profiles are shown in Figs. 4 and 5. To interpret these results, it must be taken into account that the profiles in Fig. 4, in which the TCD detector was employed, can be complicated by phenomena of desorption of CO and the opposite thermal conductivity of CO_2 formed. Nevertheless, the profile taken with QMS detection (Fig. 5) can be used for the separation of the reduction from the complicated TCD signal as well as to check the absence of generation of any residual hydrocarbons during these tests. According to the comparison between Figs. 4 and 5, part of the CO remains chemisorbed at low temperature, probably in the form of carbonate-like species as it occurs for this type of samples under CO-PROX reaction conditions [13]. In addition, in accordance to XPS results above and results obtained in previous work [20], copper can be stabilised in a Cu^+ state in this type of samples during reduction with CO. These aspects can make difficult the complete assignment of the TPR features obtained when using CO as reductant. In any case, the results (Figs. 3–5) reveal the highest reducing power of CO with respect to H_2 for these samples, in agreement with previous work [5,13]. Such difference is also in agreement with operation of the systems by means of a redox mechanism in which CO and H_2 basically compete for oxygens at the active dispersed copper oxide entities or copper oxide–ceria interfaces [6,13]. In accordance with this hypothesis, it can be noted that comparative analysis of the reduction temperatures observed during these CO-TPR experiments (Figs. 4 and 5) is also in qualitative agreement with activity results (Fig. 1). Nevertheless, the presence of interferences between the different gases present under CO-PROX conditions can be responsible of subtle differences observed between the catalytic behaviour for CO and H_2 oxidation and the behaviour observed towards reduction of the individual gases.

4. Conclusions

Differences in the catalytic activities of nanostructured systems based on combinations between oxidised copper and cerium entities for preferential oxidation of CO in a H_2-rich stream are shown to depend strongly on the specific components configuration present in each case which in turn depends on the preparation method and copper loading employed. Qualitative agreement between the reactivities observed towards the two reductants employed (CO and H_2) and the analysis of the redox behaviour of the systems towards individual interactions with the two reactants (analysed by XPS, H_2-TPR and CO-TPR) is observed, strongly suggesting the operation of the systems by means of redox mechanisms in which both reductants compete for the oxygens of the solid. In particular, the highest CO-PROX activity is observed for a system in which a strong reduction of the ceria component is apparently produced and related to the presence of highly dispersed copper oxide entities on the ceria surface. Nevertheless, establishment of a more complete correlation between redox and catalytic properties in these systems likely requires a more precise analysis of interferences between reactants in the complex CO-PROX atmosphere.

Acknowledgements

D.G. and A.H. thank the Ministerio de Educación y Ciencia (MEC) and the CSIC for a FPI PhD and I3P postgraduate grants, respectively. Thanks are due to the CICyT or MEC (projects MAT2003-03925 and CTQ2006-15600/BQU), Comunidad de Madrid (project ENERCAM S-0505/ENE/000304) and CSIC-HAS bilateral agreement for financial support.

References

[1] J.R. Rostrup-Nielsen, J. Sehested, J.K. Norskov, Adv. Catal. 47 (2002) 65.
[2] Q. Fu, H. Saltsburg, M. Flytzani-Stephanopoulos, Science 301 (2003) 935.
[3] G. Avgouropoulos, T. Ioannides, Ch. Papadopoulou, J. Batista, S. Hocevar, H.K. Matralis, Catal. Today 75 (2002) 157.
[4] S.H. Oh, R.M. Sinkevitch, J. Catal. 142 (1993) 254.
[5] J.B. Wang, S. Lin, T. Huang, Appl. Catal. A 232 (2002) 107.
[6] G. Sedmak, S. Hocevar, J. Levec, J. Catal. 213 (2003) 135.
[7] D.H. Kim, J.E. Cha, Catal. Lett. 86 (2003) 107.
[8] W.B. Kim, T. Voitl, G.J. Rodríguez-Rivera, S.T. Evans, J.A. Dumesic, Angew. Chem. Int. Ed. 44 (2005) 778.

[9] Y. Liu, Q. Fu, M. Flytzani-Stephanopoulos, Catal. Today 93–95 (2004) 241.
[10] G. Marbán, A.B. Fuertes, Appl. Catal. B 57 (2005) 43.
[11] A. Martínez-Arias, A.B. Hungría, M. Fernández-García, J.C. Conesa, G. Munuera, J. Power Sources 151 (2005) 32.
[12] F. Mariño, C. Descorme, D. Duprez, Appl. Catal. B 58 (2005) 175.
[13] A. Martínez-Arias, A.B. Hungría, G. Munuera, D. Gamarra, Appl. Catal. B 65 (2006) 207.
[14] J.-W. Park, J.-H. Jeong, W.-L. Yoon, H. Jung, H.-T. Lee, D.-K. Lee, Y.-K. Park, Y.-W. Rhee, Appl. Catal. A 274 (2004) 25.
[15] M. Jobbagy, F. Mariño, B. Schönbrod, G. Baronetti, M. Laborde, Chem. Mater. 18 (2006) 1945.
[16] A. Martínez-Arias, J. Soria, R. Cataluña, J.C. Conesa, V. Cortés Corberán, Stud. Surf. Sci. Catal. 116 (1998) 591.
[17] W. Liu, A.F. Sarofim, M. Flytzani-Stephanopoulos, Chem. Eng. Sci. 49 (1995) 4871.
[18] A. Martínez-Arias, M. Fernández-García, O. Gálvez, J.M. Coronado, J.A. Anderson, J.C. Conesa, J. Soria, G. Munuera, J. Catal. 195 (2000) 207.
[19] B. Skårman, D. Grandjean, R.E. Benfield, A. Hinz, A. Andersson, L.R. Wallenberg, J. Catal. 211 (2002) 119.
[20] A. Martínez-Arias, A.B. Hungría, M. Fernández-García, J.C. Conesa, G. Munuera, J. Phys. Chem. B 108 (2004) 17983.
[21] A.N. Ilichev, A.A. Firsova, V.N. Korchak, Kinet. Catal. 47 (2006) 585.
[22] P. Ratnasamy, D. Srinivas, C.V.V. Satyanarayana, P. Manikandan, R.S. Senthil Kumaran, M. Sachin, V.N. Shetti, J. Catal. 221 (2004) 455.
[23] M. Manzoli, R. Di Monte, F. Bocuzzi, S. Coluccia, J. Kašpar, Appl. Catal. B 61 (2005) 192.
[24] G. Avgouropoulos, T. Ioannides, H. Matralis, Appl. Catal. B 56 (2005) 87.
[25] A. Tschöpe, M.L. Trudeau, J.Y. Ying, J. Phys. Chem. B 103 (1999) 8858.
[26] P. Bera, K.R. Priolkar, P.R. Sarode, M.S. Hegde, S. Emura, R. Kumashiro, N.P. Lalla, Chem. Mater. 14 (2002) 3591.
[27] X.Q. Wang, J.A. Rodriguez, J.C. Hanson, D. Gamarra, A. Martínez-Arias, M. Fernández-García, J. Phys. Chem. B 109 (2005) 19595.
[28] W. Shan, W. Shen, C. Li, Chem. Mater. 15 (2003) 4761.
[29] D. Gamarra, A. Martínez-Arias, G. Munuera, A.B. Hungría, M. Fernández-García, J.C. Conesa, P.A. Midgley, X.Q. Wang, J.C. Hanson, J.A. Rodríguez, J. Catal., submitted for publication.
[30] A. Martínez-Arias, M. Fernández-García, V. Ballesteros, L.N. Salamanca, J.C. Conesa, C. Otero, J. Soria, Langmuir 15 (1999) 4796.
[31] R. Hesse, T. Chassé, R. Szargan, Fresenius J. Anal. Chem. 365 (1999) 48.
[32] J.P. Holgado, R. Alvarez, G. Munuera, Appl. Surf. Sci. 161 (2000) 301.
[33] P. Mars, D.W. van Krevelen, Chem. Eng. Sci. 3 (1954) 41 (special supplement).
[34] D. Gamarra, A. Martínez-Arias, in press.
[35] C.D. Wagner, Faraday Discuss. Chem. Soc. 60 (1975) 291.
[36] G. Moretti, J. Electron Spectrosc. Relat. Phenom. 95 (1998) 95.
[37] W. Grünert, N.W. Hayes, R.W. Joyner, E.S. Shpiro, J. Phys. Chem. 98 (1994) 10832.
[38] G. Munuera, in press.
[39] A. Pintar, J. Batista, S. Hocevar, J. Colloid Interface Sci. 285 (2005) 218.
[40] J.P. Holgado, G. Munuera, Stud. Surf. Sci. Catal. 96 (1995) 109.